Single-Molecule Magnets

Polyoxometalate-Mediated Self-Assembly of Single-Molecule Magnets: $\{[XW_9O_{34}]_2[Mn^{III}_4Mn^{II}_2O_4(H_2O)_4]\}^{12-}$**

Chris Ritchie, Alan Ferguson, Hiroyuki Nojiri, Haralampos N. Miras, Yu-Fei Song, De-Liang Long, Eric Burkholder, Mark Murrie,* Paul Kögerler, Euan K. Brechin, and Leroy Cronin*

Polyoxometalates (POMs), anionic oxide clusters of the early transition metals,[1] represent a vast class of inorganic materials with a virtually unmatched range of properties applicable to biology,[2] magnetism,[3] materials science,[4] or catalysis.[5] This unique span of properties qualifies POM-based materials as prime candidates for the designed construction of electronically interesting materials. Polyoxometalates possess enormous diversity in both size and structure[1b,6] and thereby provide access to a huge library of readily available and controllable fragments, that is, secondary building units (SBUs)[7] that can be interconnected by electrophiles.

The development of novel magnetic polyoxometalates[8] targets either the magnetic functionalization of the metal oxide fragment itself, which is mostly relevant for polyoxovanadates such as $\{V_{15}As_6\}$,[9] the interlinking of POM building blocks, as seen for $\{Mo_{72}Fe_{30}\}$,[10] $[PMo_{12}O_{40}(VO)_2]^{5-}$,[11] or the use of lacunary POM fragments as multidentate ligands binding to polynuclear paramagnetic coordination clusters (e.g., $\{W_{18}Cu_6\}$[12] and $\{W_{48}Cu_{20}\}$[13]). In particular, we reasoned that targeting the assembly of a mixed-valence manganese-based cluster[14–15] within a polyoxometalate ligand cage could offer many fantastic new possibilities for design and manipulation. For example, the POM "ligands" could be useful to "dilute" single-molecule magnets (SMMs) to remove unwanted dipolar interactions and also because of the intrinsic redox activity of the POM "ligands" that could allow additional routes to control

magnetic-exchange pathways or introduce other functionality for device applications.[11] In addition, the POM shells are themselves surface compatible as well as being excellent ligands and SBUs that will allow a very high degree of reliable design and assembly that is not possible to achieve in SMMs based on first-row transition metals alone.

One of the major limitations in the development of SMMs is that the underlying design strategies lie within the boundaries set by the serendipitous self-assembly of metal ions with bridging ligands of different connectivites and the controlled assembly of rigid building blocks typified by metallocyanide (Prussian blue-type) chemistry.[16] Within this scheme there have also been attempts to influence the primary SMM parameters (spin ground state and molecular anisotropy) deliberately through targeted structural and chemical modification.[17] However, despite the comparably precise structural control on the molecular level that characterizes POM chemistry, no single-molecule magnet has yet been derived from a polyoxometalate, as evidenced by hysteresis in magnetization versus field studies. Although several POM-based systems with high spin ground states or significant magnetic anisotropy are known,[18] and hybrid $[SMM]^{n+}[POM]^{n-}$ salts have been isolated,[19] a bona fide polyoxometalate-based SMM has not yet been reported.

Herein we report the first two examples of $Mn^{II/III}$-based SMMs encapsulated within a polyoxometalate ligand system derived from the trivacant lacunary $\{B-\alpha-X^{IV}W^{VI}_9O_{34}\}^{10-}$ polyanion. The resulting clusters both contain a central, mixed-valence $\{Mn_6\} = [Mn^{III}_4Mn^{II}_2O_4(H_2O)_4]^{8+}$ cluster core that is anchored between two rigid lacunary $[XW_9O_{34}]^{10-}$ polyoxometalate clusters. These species were isolated as $Na_4K(C_4H_{10}NO)_7\{[GeW_9O_{34}]_2[Mn^{III}_4Mn^{II}_2O_4(H_2O)_4]\}\cdot15H_2O$ (**1**) and $(C_4H_{10}NO)_{12}\{[SiW_9O_{34}]_2[Mn^{III}_4Mn^{II}_2O_4(H_2O)_4]\}\cdot15H_2O$ (**2**). The cluster anions in **1** and **2** are structural analogues and differ only in the heteroatoms X that are central to the $\{XW_9O_{34}\}$ fragments (X = Ge in **1**, X = Si in **2**), see Figure 1.

Compounds **1** and **2** can thus be described as two $\{B-\alpha-XW_9O_{34}\}^{10-}$ polyanions that sandwich a mixed-valence cationic hexanuclear $[Mn^{III}_4(H_2O)_2Mn^{II}_2O_4(H_2O)_2]^{8+}$ cluster. The $\{[Mn^{III}_4Mn^{II}_2O_4(H_2O)_4]\}$ cluster is a C_i-symmetric double cubane, in which each cubane comprises three Mn^{III} and one Mn^{II} center, with two of the Mn^{III} centers shared between the cubanes. Each of the Mn centers encapsulated by the trivacant B-α type lacunary ligands has three coordination bonds to the polytungstate unit; Mn—OW bonds range from 1.934(1) to 2.166(2) Å and Mn—OGe bonds are between 1.972(2) and 2.260(1) Å. As the polynuclear Mn^{III}/Mn^{II} cores

[*] Dr. C. Ritchie, Dr. A. Ferguson, Dr. H. N. Miras, Dr. Y.-F. Song, Dr. D.-L. Long, Dr. E. Burkholder, Dr. M. Murrie, Prof. Dr. L. Cronin
WestCHEM, Department of Chemistry, The University of Glasgow
University Avenue, Glasgow G12 8QQ, Scotland (UK)
Fax: (+44) 141-330-4888
E-mail: M.Murrie@chem.gla.ac.uk
         L.Cronin@chem.gla.ac.uk
Homepage: http://www.chem.gla.ac.uk/staff/lee

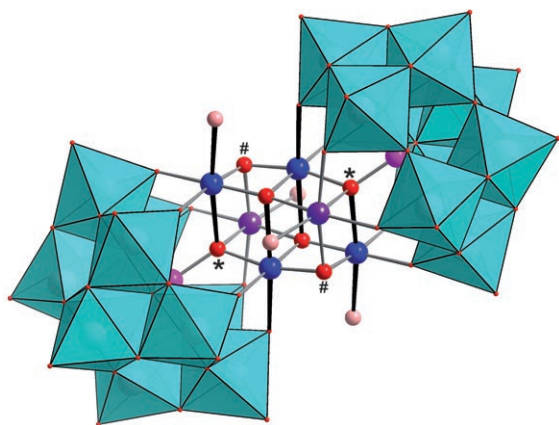Prof. Dr. H. Nojiri
IMS, Tohoku (Japan)

Prof. Dr. P. Kögerler
Institut für Anorganische Chemie, RWTH Aachen University (Germany)

Dr. E. K. Brechin
School of Chemistry, Edinburgh University (UK)

Supporting information for this article is available on the WWW under http://dx.doi.org/10.1002/anie.200801281.
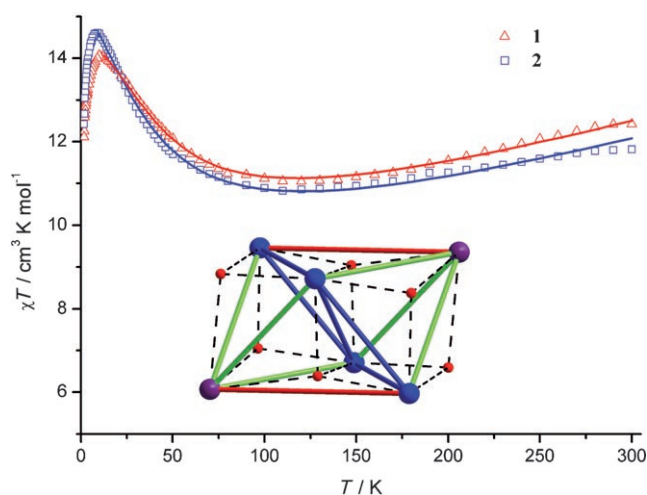
Figure 1. Representation of the [{XW$_9$}$_2${Mn$_6$}]$^{12-}$ polyanions in **1** and **2**. The polyoxotungstate fragments are shown as polyhedra, and the central {Mn$_6$O$_4$(OH$_2$)$_4$} double-cubane cluster and the connecting heteroatoms are shown as ball-and-stick (Mn^{III} blue, Mn^{II} violet, X purple, O red, H$_2$O pink, H omitted for clarity). The elongated Jahn–Teller axes of the Mn^{III} ions are shown in black.

Figure 2. Temperature dependence of $\chi_M T$ for **1** (red triangles) and **2** (blue squares) from 300–1.8 K at 0.1 T. Solid lines represent best fits to a Heisenberg-only model ($T > 15$ K, see text). Inset: Exchange connectivity within the Mn$_6$O$_6$ double-cubane core (Mn^{II} violet spheres, Mn^{III} blue spheres, all other corners/intersections represent μ-oxo groups) illustrating the three principal superexchange pathways: J_1 (Mn^{II}–Mn^{III}, green lines), J_2 (Mn^{III}–Mn^{III}, blue lines), and J_3 (Mn^{II}–Mn^{III}, red lines).

found in **1** and **2** are chemically equivalent, it is intriguing to note that the geometry of the core is strongly affected by the POM ligand to which it is attached. Indeed it is the differing lengths of the Ge−O (1.733(1) Å) and Si−O (1.623(1) Å) bonds in the respective lacunary clusters that have the most significant impact, as it is these bonds that dictate the dimension of the {Mn$_6$} core trapped between the polytungstate ligands. The net effect is a contraction of 0.22 Å in the {Mn$_6$} core of **1** relative to **2** when measuring between the symmetry related O* ligands as seen in Figure 1. Further, the bond lengths and angles within the cores of **1** and **2** also vary, specifically the bonds running parallel to the aligned Jahn–Teller axes of the four Mn^{III} ions. The most significant structural difference within the Mn$^{II/III}$ cores of **1** and **2** are the respective O*-Mn-O$^{\#}$ linkages with bond lengths of 1.972(1) and 1.870(1) Å in **1** and 1.988(1) and 1.856(2) Å in **2**. Accompanying these variations in bond lengths is a greater than 2.5° difference in the corresponding bond angles of O*-Mn-O$^{\#}$ between **1** and **2** (165.8° and 168.1°).

The room-temperature $\chi_M T$ value of 12.4 cm^3 K mol^{-1} for **1** is lower than the spin-only ($g = 2$) value for a {Mn^{III}$_4$Mn^{II}$_2$} unit (20.75 cm^3 K mol^{-1}). The value of $\chi_M T$ slowly decreases upon cooling to around 120 K, where it reaches a minimum value of 11 cm^3 K mol^{-1} before increasing to a maximum of 14.1 cm^3 K mol^{-1} at 10 K. The $\chi_M T$ value sharply decreases below this temperature. Compound **2** shows similar behavior; a value of 11.8 cm^3 K mol^{-1} is observed at room temperature and a maximum value of 14.6 cm^3 K mol^{-1} at 9 K, followed by a sharp decrease (Figure 2).

For both complexes, this behavior is indicative of the presence of competing ferro- and antiferromagnetic exchange interactions between the metal centers, and the low-temperature maximum is indicative of a ground state with $S = 5$. The low-temperature (< 10 K) decrease is assigned to zero-field splitting, intermolecular interactions, and the Zeeman effects of the applied field. The small differences in the $\chi_M T$ curves above 10 K are consistent with the small change in Mn-O-Mn

bridging angles between the two structures, related to the structural differences of either Ge or Si at the edges of the {Mn$_6$} core. To establish the effects of these structural differences, a simplified spin Hamiltonian, based solely on isotropic Heisenberg-type exchange, was used to model the susceptibility data above 15 K (to avoid zero-field-splitting effects). In a first approximation, three types of nearest-neighbor coupling can be identified: 1) coupling between Mn^{II} and Mn^{III} centers through two μ-oxo groups and Mn-O-Mn angles of approx. 90°, 2) similar Mn^{III}(μ-O)$_2$Mn^{III} pairs, and 3) Mn^{II}-O-Mn^{III} pairs with Mn-O-Mn angles close to 180°, causing strong antiferromagnetic coupling (Figure 2). A least-squares fit yields $J_1 = 6.5$ cm^{-1}, $J_2 = 3.5$ cm^{-1}, $J_3 = -56.0$ cm^{-1} for **1** and $J_1 = 5.5$ cm^{-1}, $J_2 = 4.5$ cm^{-1}, $J_3 = -59.5$ cm^{-1} for **2** (common $g_{iso} = 2.0$, Figure 2).

To further verify the magnitude of the spin ground state for complexes **1** and **2**, magnetization data were collected in the ranges 1–5 T and 1.8–7.0 K and these are plotted as reduced magnetization ($M/N\beta$) versus H/T in Figure S3 (see the Supporting Information). For a complex entirely populating the ground state and experiencing no zero-field splitting, the observed isofield lines should superimpose and saturate at a value ($M/N\beta$) equal to gS. The fitting of the experimental data with the axial ZFS plus Zeeman Hamiltonian[20] given in Equation (1) over the whole field and temperature range afforded the parameters: **1**: $S = 5$, $g = 1.94$, $D = -0.67$ cm^{-1} and **2**: $S = 5$, $g = 1.99$, $D = -0.62$ cm^{-1}.

$$\hat{H} = D(\hat{S}_z{}^2 - S(S+1)/3) + \mu_B g H \hat{S} \tag{1}$$

Given the magnitude of S and the sign of D, ac susceptibility studies were performed to see if complexes **1** and **2** indeed exhibit SMM characteristics (see Figure S2 in

the Supporting Information). The sharp decrease in $\chi_M T$ below 10 K observed in the dc measurements is present in the ac measurements, and is more pronounced for higher frequencies. Below 5 K, the $\chi' T$ curves for the different frequencies start to diverge, and a concomitant frequency-dependent χ'' signal is observed. For **1**, well-resolved peaks in χ'' are seen above 1.8 K and an Arrhenius analysis yields the parameters: $\Delta E/k_B = 14.8$ K (10.3 cm^{-1}) and $\tau_0 = 3.1 \times 10^{-7}$ s. The former value is lower than the theoretical barrier of 24 K obtained from S and D parameters as derived from fitting the reduced magnetization. The C_i point symmetry of the {Mn$_6$} core leads to transverse anisotropy terms in the ZFS Hamiltonian, reducing the effective height of the energy barrier separating the $\pm M_S$ states, through quantum tunneling of magnetization (Figure 3).
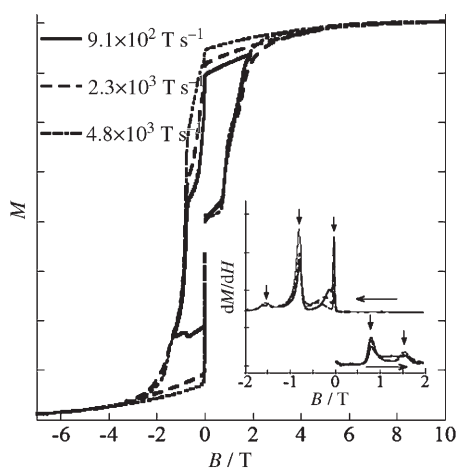
Figure 3. Pulsed-field measurements for **1** at 0.5 K. Three measurements at different sweep rates are shown. Inset: Derivative plot showing five peaks equally spaced around 0.78 T apart.

HF-EPR and INS (inelastic neutron scattering) experiments are planned to determine the spin-Hamiltonian parameters more accurately. For **2**, no peaks in χ'' are seen above 1.8 K, indicating a lower energy barrier to reorientation of the magnetization, which is consistent with the smaller D value. To examine the relaxation behavior of compound **1**, pulsed-field measurements were performed for different sweep rates at 1.6 and 0.5 K (see Figure S3 in the Supporting Information). The complex shows temperature- and sweep-rate-dependent magnetic hysteresis with steplike features (five peaks with an equal spacing between the peaks of ca. 0.78 T), which correspond to the adiabatic quantum-tunneling transitions expected for a genuine SMM. These features equate to increased magnetization relaxation, which is indicative of quantum tunneling of magnetization (QTM) between the $\pm Ms$ levels on opposite sides of the anisotropy barrier. The separation between the steps is related to D by the equation $\Delta H = |D|/g\mu_B$. Measurement of the step positions for complex **1** affords an average field separation of approximately 0.78 T and thus a $|D|/g$ value of about 0.35 cm^{-1}. Assuming $g = 2.00$, this corresponds to a $|D|$ value of approximately 0.71 cm^{-1}, which is in excellent

agreement with that obtained from the dc magnetization measurements (0.67 cm^{-1}).

In summary we have shown that it is possible to embed a mixed-valence {Mn$^{III}_4$Mn$^{II}_2$} unit within a set of lacunary polyoxometalate {B-α-XW$_9$O$_{34}$}$^{10-}$ polyanions and that these ligands are able to effectively isolate the Mn metal–oxo core. The rather complex and distorted nature of the cationic core shows the fascinating ability of polyanion ligands to cap metal clusters such as these despite their rigid structures and to stabilize even distorted coordination configurations. Additionally, the involvement of the tetrahedral oxo ligands is essential for completing the coordination environment of the encapsulated transition metals, and they also act as ideal tunable units to modify the physical properties of the molecules. It is the combination of these parameters that allows the fine tuning of the magnetic properties of the clusters. In further work we will extend this approach to isolate a range of nuclearity cores of various symmetries with the aim of providing redox-POM-based SBUs (with the ability to add organic linkers) that can be used to discover, design, and systematically tailor new SMMs with a large degree of control.

Experimental Section

[1] a) D.-L. Long, E. Burkholder, L. Cronin, *Chem. Soc. Rev.* **2007**, *36*, 105; b) L. Cronin, *Comprehensive Coordination Chemistry II*, Vol. 7 (Eds.: J. A. McCleverty T. J. Meyer), Elsevier, Amsterdam, **2004**, pp. 1–57; c) *Polyoxometalate Chemistry: From topology via self-assembly to applications* (Eds.: M. T. Pope, A. Müller), Kluwer, Dordrecht, **2001**.

[2] a) B. Hasenknopf, *Front. Biosci.* **2005**, *10*, 275; b) D. A. Judd, J. H. Nettles, N. Nevins, J. P. Snyder, D. C. Liotta, J. Tang, J. Ermolieff, R. F. Schinazi, C. L. Hill, *J. Am. Chem. Soc.* **2001**, *123*, 886; c) J. Schemberg, K. Schneider, U. Demmer, E. Warkentin, A. Müller, U. Ermler, *Angew. Chem.* **2007**, *119*, 2460; *Angew. Chem. Int. Ed.* **2007**, *46*, 2408.

[3] a) A. Müller, P. Kögerler, A. W. M. Dress, *Coord. Chem. Rev.* **2001**, *222*, 193; b) T. Yamase, K. Fukaya, H. Nojiri, Y. Ohshima, *Inorg. Chem.* **2006**, *45*, 7698.

[4] a) D.-L. Long, H. Abbas, P. Kögerler, L. Cronin, *Angew. Chem.* **2005**, *117*, 3387; *Angew. Chem. Int. Ed.* **2005**, *44*, 3323; b) C. Streb, D.-L. Long, L. Cronin, *Chem. Commun.* **2007**, 471; c) H. Zeng, G. R. Newkome, C. L. Hill, *Angew. Chem.* **2000**, *112*, 1841; *Angew. Chem. Int. Ed.* **2000**, *39*, 1771.

[5] a) J. T. Rhule, W. A. Neiwert, K. I. Hardcastle, B. T. Do, C. L. Hill, *J. Am. Chem. Soc.* **2001**, *123*, 12101; b) M. V. Vasylyev, R. Neumann, *J. Am. Chem. Soc.* **2004**, *126*, 884; c) N. Mizuno, K. Yamaguchi, K. Kamata, *Coord. Chem. Rev.* **2005**, *249*, 1944.

[6] D.-L. Long, L. Cronin, *Chem. Eur. J.* **2006**, *12*, 3698.

[7] a) M. Eddaoudi, D. B. Moler, H. Li, B. Chen, T. M. Reineke, M. O'Keeffe, O. M. Yaghi, *Acc. Chem. Res.* **2001**, *34*, 319; b) S. L. James, *Chem. Soc. Rev.* **2003**, *32*, 276.

[8] A. Müller, F. Peters, M. T. Pope, D. Gatteschi, *Chem. Rev.*, **1998**, *98*, 239.

[9] D. Gatteschi, L. Pardi, A. L. Barra, A. Müller, J. Döring, *Nature* **1991**, *354*, 463.

[10] A. Müller, M. Luban, C. Schröder, R. Modler, P. Kögerler, M. Axenovich, J. Schnack, P. Canfield, S. Bud'ko, N. Harrison, *ChemPhysChem* **2001**, *2*, 517.

[11] J. Lehmann, A. Gaita-Arino, E. Coronado, D. Loss, *Nat. Nanotechnol.* **2007**, *2*, 312.

[12] T. Yamase, K. Fukaya, H. Nojiri, Y. Ohshima, *Inorg. Chem.* **2006**, *45*, 7698.

[13] S. S. Mal, U. Kortz, *Angew. Chem.* **2005**, *117*, 3843; *Angew. Chem. Int. Ed.* **2005**, *44*, 3777.

[14] Z. Zhang, E. Wang, W. Chen, H. Tan, *Aust. J. Chem.* **2007**, *60*, 284.

[15] A. J. Tasiopoulos, A. Vinslava, W. Wernsdorfer, K. A. Abboud, G. Christou, *Angew. Chem.* **2004**, *116*, 2169; *Angew. Chem. Int. Ed.* **2004**, *43*, 2117.

[16] J. N. Rebilly, T. Mallah, *Struct. Bonding (Berlin)* **2006**, *122*, 103.

[17] See for example: a) N. Ishikawa, M. Sugita, T. Ishikawa, S. Koshihara, Y. Kaizu, *J. Am. Chem. Soc.* **2003**, *125*, 8694; b) C. J. Milios, R. Inglis, A. Vinslava, R. Bagai, W. Wernsdorfer, S. Parsons, S. P. Perlepes, G. Christou, E. K. Brechin, *J. Am. Chem. Soc.* **2007**, *129*, 12505; c) G. Aromí, E. K. Brechin, *Struct. Bonding (Berlin)* **2006**, *122*, 1.

[18] J. M. Clemente-Juan, E. Coronado, *Coord. Chem. Rev.* **1999**, *193*, 361; B. Botar, P. Kögerler, A. Müller, R. Garcia-Serres, C. L. Hill, *Chem. Commun.* **2005**, 5621.

[19] A. Forment-Aliaga, E. Coronado, M. Feliz, A. Gaita-Arino, R. Llusar, F. M. Romero, *Inorg. Chem.* **2003**, *42*, 8019.

[20] S. Piligkos, E. Bill, D. Collison, E. J. L. McInnes, G. A. Timco, H. Weihe, R. E. P. Winpenny, F. Neese, *J. Am. Chem. Soc.* **2007**, *129*, 760.